Sensors & Diagnostics

PAPER

View Article Online
View Journal

Cite this: DOI: 10.1039/d6sd00030d

Highly sensitive pH-modulated paper-based platform for point-of-care osteopontin quantification in osteoporosis screening

Amandeep Kaur, [ab] Vikas, [ab] Sanjeev Soni[ab] and Suman Singh*[ab]

This work presents the development of paper-based colorimetric biosensors for the detection of the osteoporosis biomarker osteopontin (OPN), which can be used for point-of-care analysis. For this purpose, simple filter paper has been used, on which test zones are printed using a conventional office desktop printer. The paper was chemically modified with glutaraldehyde to create binding sites for gold nanoparticle-conjugated antibodies. The surface modification was confirmed by Fourier-transform infrared spectroscopy (FTIR). Colorimetric detection was performed using phenol red as a pH-sensitive sensor probe, and this sensitivity was visualised by the immediate generation of brick red color in the test zone of the biosensor upon immunocomplex formation between antibody-conjugated gold nanoparticles and the osteopontin biomarker. The color intensity was quantified using reflectance spectroscopy and the RGB coordinate provided by the ImageJ Program from the photograph taken with a smartphone camera. The sensor demonstrated good noticeable sensitivity in the range of 1–125 ng mL^{-1} ($R^2 > 0.99$) in buffer and in the range of 1–100 ng mL^{-1} ($R^2 > 0.957$) with a detection limit of 0.52 ng mL^{-1} in buffer and 0.48 ng mL^{-1} in commercial human sera solution. The detection is possible within 15 minutes of reaction time. In addition, this biosensor shows good selectivity toward other interfering biomarkers, such as bovine serum albumin, osteocalcin, and CTX-1. The developed assay meets the criteria of being easy to use, affordable, and time-saving and requiring a smaller sample volume, which is beneficial for future screening and detection of osteoporosis.

Received 6th February 2026,
Accepted 5th May 2026

DOI: 10.1039/d6sd00030d

rsc.li/sensors

1 Introduction

Osteoporosis is a bone disease that reduces bone strength and density, causing bones to become weaker and brittle. It increases the risk of fractures in some peripheral joints, hips, and spinal vertebrae. Although it affects both genders, it occurs more predominantly in women. According to the report by the International Osteoporosis Foundation (IOF), approximately 44 million people suffered from osteoporosis fractures in the United States, and 200 million experienced fractures worldwide.[1] In India, around 50 million people suffer from either osteoporosis (T-score > 2.5) or have a lesser bone mass ranging from 1 to 2.5 T-score.[2] The existing conventional diagnostic methods include measurement of bone mineral density (BMD),[3] dual energy X-ray absorptiometry (DXA),[3] ELISA (enzyme linked sorbent immunoassay),[4] RIA (radioimmunoassay), *etc.* Most of these technologies are costly, time-consuming, and require expertise. Therefore, there is an urgent need for early detection methods that are cost effective and robust, and easy to use point-of-care diagnostic methods for osteoporosis biomarker detection, requiring not much skill. In addition to these conventional techniques, a bone turnover biochemical marker may also reflect the status of bone metabolism. Several markers like osteocalcin (OCN),[5] osteopontin (OPN),[6] C-terminal cross-linked telopeptide of type 1 collagen (CTX-1),[3] *etc.* have been widely used for the sensitive and selective assessment of bone health.

Osteopontin (OPN) in blood serum has been used as a potential biomarker for clinical diagnosis and cancer treatment.[7] It plays a vital role in the regulation of bone metabolism through the sympathetic nervous system.[8] OPN not only regulates bone mass, but also takes part in various biological activities, promoting proliferation, migration, and adhesion of bone cells to maintain bone homeostasis.[8] It also demonstrates a significant correlation with bone-related diseases such as osteoporosis, rheumatoid arthritis, and osteosarcoma, with its overexpression indicating the risk for osteoporosis.[9] This correlation between OPN and osteoporosis has gained more attention in the recent past in determining the severity of the disease.[6,10,11]

For point-of-care applications, researchers have come up with many sensing platforms for the estimation of osteoporosis

[a] CSIR-Central Scientific Instruments Organisation, Sector 30-C, Chandigarh 160030, India. E-mail: ssingh@csio.res.in
[b] Academy of Scientific and Innovative Research (AcSIR), Ghaziabad 201002, India

biomarkers, like an electrochemical sensing platform,[12,13] ELISA-based immunoassays, *etc.* Immunoassays such as immuno-radiometric assay (IRMA) and enzyme immunoassay have been reported for bovine osteocalcin (OCN) which shares 90% homology with human OCN.[14,15] Similarly, in order to reduce the complexity of the protocol, an electrochemical-based interdigital electrode (IDE) sensor is developed for the quantification of the CTX-1 biomarker.[16] The sensor consisted of a gold nanoparticle-modified anti-CTX-1 antibody attached to a silica nanomaterial-based IDE, capable of quantifying CTX-1 as low as 0.5 pg mL^{-1} through interactions.[17] Another study reported the development of a simple electrochemical immunosensor with a gold nanoparticle electrodeposited on a chitosan-reduced graphene oxide composite modified electrode for the determination of bone gamma-carboxyglutamate (BGP), ranging from 100 ag mL^{-1} to 10 μg mL^{-1}, with a limit of detection (LOD) of 20 ag mL^{-1} in human serum.[18] A study based on the development of an immunological biosensor-based electrochemical impedance spectroscopy system provides a quantitative measurement of osteocalcin, exhibiting an LOD of 10–60 pg μL^{-1} with a response time of 45 minutes.[19] Chinnappan *et al.*,[20] reported an aptamer-based sensor for the detection of osteocalcin (OCN) and a beta-crosslap (BC) bone density biomarker with a binding affinity (K_d) of 59 nm and 55 nm, respectively, with the detection limits of OCN and BC found to be 0.4 pg mL^{-1} and 0.21 pg mL^{-1}, respectively. Chung *et al.* reported a quartz-crystal microbalance (QCM) biosensor for detecting TRAP 5a, TRAP 5b, or the total TRAP concentration in blood samples. It was captured by the antibodies immobilized on the cantilever surface, which was then measured using an optical detection plate.[21] Zhang *et al.* presented a label-free electrochemical method for studying ALP activity based on the difference in the surface charge of electrodes. Phosphorylated peptides were immobilized on the surface of gold electrodes to make negatively charged self-assembled monolayers (SAMs) interfacing with $[Ru(NH_3)_6]^{3+}$ probes for electrochemical sensing.[22] Hsieh *et al.* designed a piezoelectric sensor for measuring the sheer stress of a knee prosthesis based on a micro-electro-mechanical system (MEMS) that transforms the stress into voltage. The sensor demonstrated a sensitivity of 0.13 mV mA^{-1} MPa^{-1} and was capable of detecting a shear force of 1.4 N.[23] However, the disadvantages associated with cross-reactivity highlight the necessity for developing biosensors that are both cost-effective and highly accurate.

In recent years, paper-based biosensors have offered a promising alternative for creating diagnostic devices, owing to their unique properties of good porosity and efficient fluid wicking capabilities. Paper is relatively cheaper, portable and easy to use, making these biosensors affordable and ready to use as a point of care device for diagnosis purposes.[24–26] Pereira *et al.* developed paper-based colorimetric sensors for osteopontin including an aptamer requiring heating before immobilization on paper employing smartphone RGB analysis[27] and an LOD below 5 ng mL^{-1} in 30 min. Similarly, Shi *et al.* introduced AuNP-based plasmonic colorimetric systems that have also been explored[28] to detect furin using G quadraplex DNAase for enhanced peroxidase-mimicking activity on ABTS, producing a green color shift. However, these approaches primarily rely on aggregation-induced optical changes. In contrast, the present study introduces a pH-responsive colorimetric immunosensor based on an OPN–AuNP@Ab interaction *via* glutaraldehyde on a paper surface, utilizing a pH-responsive phenol red mechanism with a detection time of 10–15 minutes without a complex procedure. A paper based microfluidic μPAD colorimetric platform has been designed for the detection of three important bone biomarkers named as vitamin D, calcium, and alkaline phosphatase, respectively.[29] μPAD images were captured using a smartphone and compared with a calibration curve for the quantification of analytes. Another study reported a nitrocellulose membrane based immunoassay platform for the detection of ovarian cancer biomarker alpha-fetoprotein (AFP) and mucin-16 (MUC16). The gold nanoparticles (AuNPs) functionalised with a cysteamine antibody complex are used for monitoring sensing signals w.r.t. change in color of AuNPs, which was further processed using ImageJ software. The limit of detection (LOD) for the AFP was calculated as 1.054 ng mL^{-1} and 0.413 ng mL^{-1} for MUC16, respectively.[30]

According to a prior article, the above reported biosensors, such as ELISA and electrochemical sensors, exhibit high sensitivity but are hampered by complex protocols, high costs, and cross-reactivity, limiting their use in point-of-care settings. DEXA is also considered the gold standard for the diagnosis of osteoporosis, as it detects bone loss following structural deterioration. However, it requires large, expensive, and high-quality imaging equipment, making large-scale screening difficult, with no information about the biochemical bone biomarkers. Additionally, it indicates that the majority of the detection methods outlined are primarily based on electrochemical principles, with limited colorimetric sensing devices for the diagnosis of osteoporosis diseases. In contrast, there is a need for a new sensor which overcomes the limitation of these existing technologies. So, our present work developed a paper-based AuNP colorimetric sensor that offers a simple, rapid, and cost-effective alternative, utilizing a pH-responsive phenol red mechanism and AuNP-conjugated osteopontin-specific antibodies for better selectivity. This design enables quick detection in minutes and is suitable for large-scale screening, particularly in resource-limited environments. While DXA remains the gold standard for diagnosis, this sensor holds promise for early-stage screening and timely intervention.

2 Experimental section

2.1. Reagents and equipment

All reagents used are of analytical grade, and all aqueous solutions were prepared in Milli-Q water. Human osteopontin (OPN) and osteopontin (OPN) detection antibodies, tri-sodium citrate, chloroauric acid, phosphate saline buffer, EDC (ethyl(dimethylamino propyl) carbodiimide), NHS (*N*-hydroxysuccinimide), glutaraldehyde, bovine serum albumin (BSA), type 1 collagen cross-linked C-telopeptide (CTX-1), and

osteocalcin (OCN) were procured from Sigma Aldrich (USA), phenol red [PR] was acquired from Loba Chemme and 96 well round bottom plates were procured from M/s SPL, Life Sciences. The paper biosensor is fabricated from filter paper, grade no. 1 filter paper (Whatman™), wherein the sensor array was printed using a general desktop printer (Canon). The schematic of the biosensor was made in Biorender software (freely available).

The absorbance studies of the sample were done on a UV-visible spectrometer (Hitachi, model U3900H, Japan), the functional group analysis was done by Fourier transform infrared spectroscopy (FTIR) (Jasco FTIR-4×), the morphology of the nanomaterial was recorded on a transmission electron microscope (TEM) (FEI, Model TECNAI G2F-20, USA), and dynamic light scattering (DLS) (Malvern Metasizer, Nano ZS90 Model) was used for the determination of size distribution and zeta potential measurement. The in-house developed reflectance spectroscopy setup was used to record the reflected light intensity from the test zone of the paper biosensor to have a quantitative estimation of the biomarker. The obtained colour intensity was quantified using ImageJ software (an open-source image processing tool), which calculated the mean of RGB values for each time point. For this, after the reaction is complete, a high-resolution image is captured using a smartphone camera (Motorola 40 Edge) and imported into ImageJ software for analysis. During the image-capturing process, consistent lighting conditions and a fixed distance are maintained to ensure optimal image quality. A region of interest was manually selected to ensure maximum accuracy. The software's Measure function was employed to extract the color mean value, particularly from the RGB channels.

2.2. Experimental methods

2.2.1 Synthesis of AuNPs by a chemical method. The monodispersed gold nanoparticles were synthesized *via* the conventional citrate base reduction method, wherein a total of 50 mL of 1 mM chloroauric acid solution ($HAuCl_4$) was boiled in a glass flask at 50 °C, with continuous stirring. 1% tri-sodium citrate was then added to this boiled solution, the consequence of which the solution color changed from black to red wine colour within 2–3 min, confirming the successful synthesis of gold nanoparticles (AuNPs).[31] AuNPs were stored under refrigerated conditions till further use.

2.2.2 Functionalization of AuNPs with detection antibodies. The nanoparticles were functionalized with osteopontin detection antibodies (10 μg mL^{-1}) using EDC chemistry, which involved the formulation of EDC (1-ethyl-3-(3-dimethylaminopropyl)carbodiimide) and NHS (*N*-hydroxysuccinimide)[30] in a 5 : 1 ratio with the nanoparticle solution. The solution was stirred continuously for 2 hours to allow proper mixing of the ingredients, and then the antibody solution was added to the mixture and incubated overnight at 4 °C. The obtained solution (AuNP@Ab conjugates and bare AuNPs) was characterized using a UV-vis spectrophotometer and transmission electron microscope (TEM). Size distribution and zeta potential measurements were performed using dynamic light scattering (DLS) (Malvern Metasizer, Nano ZS90 Model).

2.2.3 Protocol for optical sensing. Prior to developing the paper-based biosensor's sensing mechanism, optical studies were conducted using UV-vis spectroscopy. For that, the pH sensitivity of each component used in the proposed sensing platform was assessed by recording an absorbance spectrum. Phenol red exhibited absorbance peaks at 431 nm & 560 nm, with the 560 nm peak considered as a signal marker. Sensor components included phenol red (PR), glutaraldehyde (Glu), AuNPs, phenol red combined with glutaraldehyde (PR-Glu), phenol red with gold nanoparticles (PR-AuNPs), phenol red combined with Glu-AuNP@Ab and phenol red combined with Glu-AuNP@Ab & osteopontin antigen (PR-Glu-AuNP@Ab-OPN). With the subsequent addition of components, the peak intensity of the phenol red solution at 560 nm shifts due to sensitivity.

2.2.4 Paper fabrication. The paper biosensor fabrication began with the design of a biosensor comprising a hydrophilic zone (detection) and a hydrophobic zone, as shown in Fig. 1a. This design was then printed on the Whatman filter paper, grade 1, using a desktop office printer with a black cartridge, and was baked in an oven at 120 °C for 10 min. The paper was cooled and is ready to use after drying at ambient temperature.

2.2.5 Paper functionalization and parameter optimization. The very first step involved the activation of the paper biosensor, followed by the addition of 10 μL glutaraldehyde solution (0.05%), freshly prepared in 50 mM PBS buffer, pH 7.4, to create the base for the immobilisation of the AuNP@Ab conjugate. The biosensor was washed with DI water 3–4 times to remove unreacted glutaraldehyde. The glutaraldehyde-treated paper provides functional group accessibility for the binding of a nanoparticle-conjugated antibody on its surface. It binds to the antibody *via* the amine or carboxylic group on the antibody's surface. The paper functionalized with glutaraldehyde was dried in an oven at 50 °C for 1 h for immobilization.

The assay was optimised for various other parameters like temperature variation (16 °C, 25 °C, 37 °C, 55 °C), biomarker concentration (1–125 ng mL^{-1}), pH variation (pH 4–8), and incubation time (5–25 minutes), and the effect is discussed in the results and discussion section.

2.2.6 Detection assay in buffer and human serum. Once all parameters were optimised, these paper biosensors were tested for analysis in buffer and in commercial human serum spiked samples. For this, the optimal selected concentration of 10 μL AuNP@Ab (1 μg mL^{-1}) conjugate was dropped onto the glutaraldehyde-functionalized paper strip and incubated for 30 minutes at room temperature. The paper was washed thrice with DI water to remove unbound conjugates. A standard solution of the osteopontin biomarker, ranging from 1 to 125 ng mL^{-1}, was prepared in PBS 7.4 and 1–100 ng mL^{-1} spiked in commercial human serum (sigma) for OPN detection. Then, 10 μL of each solution was dropped

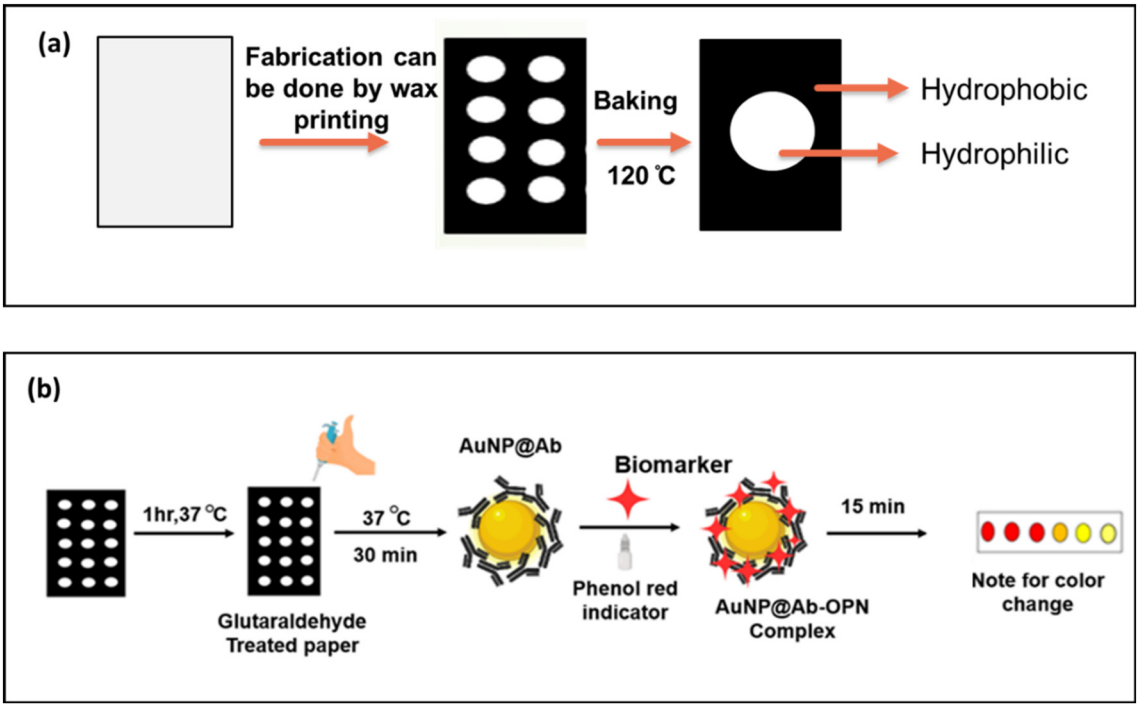

Fig. 1 Schematic of (a) paper biosensor fabrication and (b) its application as a colorimetric sensor.

onto the paper sensor and incubated for 15 minutes at room temperature. Lastly, 2 μL phenol red dye was added, which is used as a pH-sensitive probe in this work. Color change was observed after 10–15 min, coinciding with the pH change upon formation of the immunocomplex, as shown in the schematic in Fig. 1b. The pictures from the test zone were taken while maintaining a fixed distance, in a black chamber. The selected colored area of interest was evaluated in ImageJ and reflectance measurement (discussed in section 2.2.7). The values of the characteristic coordinates provided by ImageJ were evaluated, and the mean color value was plotted against OPN concentration to obtain a linear graph analysis, which was used to make a quantitative estimation.

2.2.7 Development of an in-house reflectance measurement setup. The measurement of the spectral variation in reflected light from a paper-based colorimetric biosensor was performed by using an in-house developed reflectance measurement setup. A uniform illumination sphere light source (UIS-LS, StellarNet, Inc., USA) having a full UV-vis wavelength range was used to excite the sample. The output of the light source was coupled into a bifurcated fibre (BFY400HF2, Thorlabs, USA) through an integrated sphere. Furthermore, spectral acquisition was conducted using a Stellarnet BlueWave miniature spectrometer (Stellarnet Inc., USA), which has a suitable spectral range for the visible region. Paper-based strips were placed on a non-reflective black plate to minimize the ambient light interference. The reflectance spectra were recorded between wavelengths of 450 and 700 nm, with particular attention to the changes in the absorption peak between 510 and 550 nm corresponding to colorimetric changes occurring due to binding with the target biomarker. The alignment and separation of the probe from the sensor were maintained constant for all measurements, which were performed under controlled ambient illumination. The schematic of the measurement setup of the spectral variation in reflected light from a paper-based colorimetric biosensor is shown in Fig. 2.

2.2.8 Selectivity study. To assess the selective detection of osteopontin (OPN), other interfering osteoporosis biomarkers, such as osteocalcin, C-terminal collagen peptide (CTX-1), and BSA, were selected for a selectivity study. The same detection protocol was applied as described in section 2.2. Each of the other interfering biomarkers was incubated to evaluate color development. For data analysis, the color coordinates were evaluated using the same ImageJ software and plotted to compare with the target OPN biomarker.

3 Results & discussion

3.1. Morphology and size distribution study of AuNPs & AuNP@Ab

The TEM imaging of AuNPs clearly showed nearly spherical, monodispersed gold nanoparticles with a diameter of approximately 25.86 nm (Fig. 3a), which, after conjugation, increased to 32.16 nm by approximately 7 nm (Fig. 3b), indicating the formation of a thin organic corona layer. The results were consistent with those of UV-vis absorption spectra.

In addition to TEM imaging, dynamic light scattering (DLS) measurements were performed using a ZetaSizer to determine particle size and charge distribution. DLS measurements confirmed that the average sizes of the nanoparticles were 36.45 nm and 49.09 nm after conjugate formation (Fig. 3c and d),

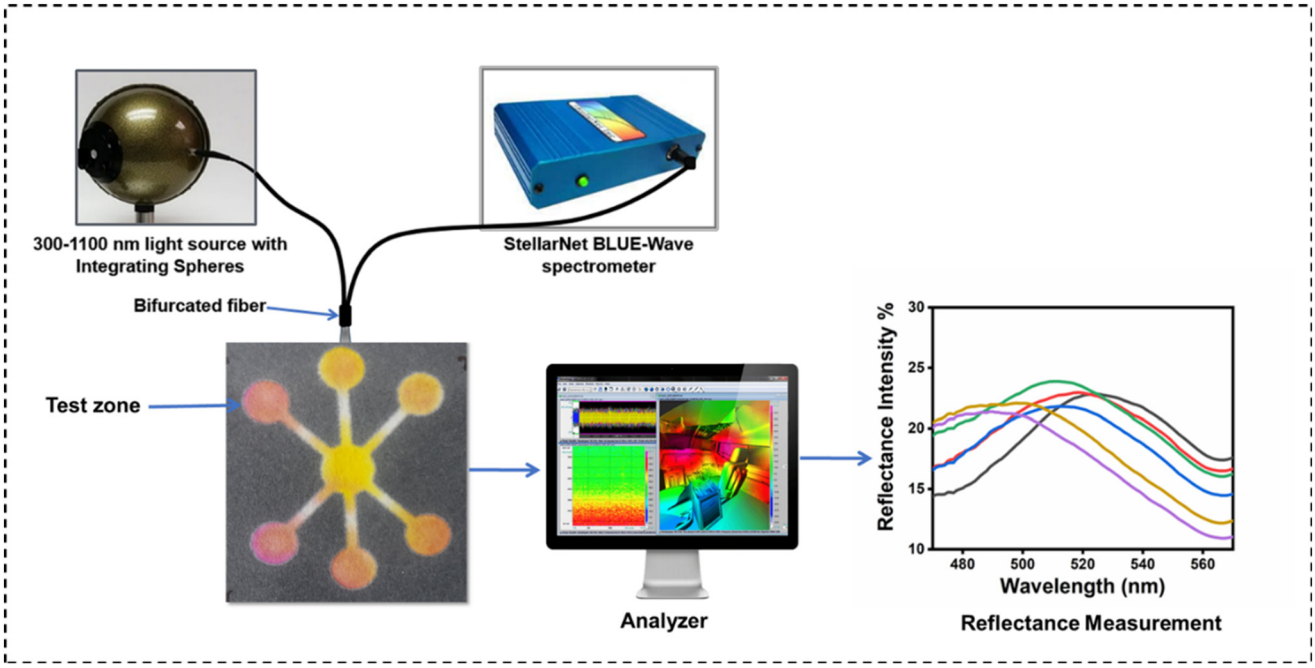

Fig. 2 Schematic of the measurement setup of the spectral variation in reflected light from the paper-based colorimetric biosensor.

with surface charges of −13.4 mV and −7.20 mV before and after the conjugation (Fig. 3e and f). Bare AuNPs typically has more negative surface charge due to the presence of stabilizing agents (citrate ions). Upon conjugation, the surface chemistry of the nanoparticles is altered due to the antibody binding of the amino acid molecule. This change partially neutralized the negative charge of the nanoparticle, and a reduction in zeta potential from −13.4 mV to −7.20 mV indicates successful binding of the antibody to the gold nanoparticles. While this reduces electrostatic repulsion, the nanoparticles remain stable due to steric stabilization from the antibodies themselves. DLS shows an expected size from 36.45 to 49.09 nm with a PDI value of 0.5 after conjugation, confirming controlled conjugation, no aggregation and instability. The hydrodynamic diameter of gold nanoparticles after conjugation is attributed to the surface-bound molecular layer and hydration shell; both factors contribute to the larger size detected by DLS. The TEM image provides a direct view of a particular nanoparticle, measuring its physical and core diameters, whereas DLS measures the hydrodynamic diameter.

3.2. Spectroscopic studies

The optical properties of gold nanoparticles were investigated using UV-visible spectroscopy. The successful synthesis of gold nanoparticles was confirmed by the change in the precursor solution color to a wine-red appearance and the presence of a surface plasmon resonance (SPR) peak at 527 nm, indicating particle sizes in the range of 10–20 nm (ref. 32) as shown in Fig. 4a. Further, the optical properties of the prepared gold nanoparticles and the conjugates were evaluated using UV-visible spectroscopy, wherein the absorbance was measured from 250 to 800 nm. Gold nanoparticles demonstrated the presence of an absorbance peak at 527 nm, which later shifted towards a higher wavelength at 533 nm upon conjugate formation with antibodies, indicating an increase in particle size due to the agglomeration phenomenon which is obvious when any conjugate is made.[33] This red shift (to a longer wavelength) is due to a change in the local refractive index around each nanoparticle. Time also played a crucial role in ensuring the dispersity of the gold nanoparticles, and it took about 30 minutes of reaction to complete, as could be visualised through the change in the color of the reaction solution (Fig. 4b).

The study of the presence of functional groups is done by recording the FTIR spectrum of AuNPs. The spectrum showed the presence of vibration stretching at 3430 cm^{-1} (O–H stretching), 2922 cm^{-1} (C–H stretching alkane), 2854 cm^{-1} (C–H stretching aldehyde), 1629 cm^{-1} (C═C stretching alkane), 1386 cm^{-1} (O–H bending) and 1033 cm^{-1}, 1033 cm^{-1} (C–O stretching), respectively, as shown in Fig. 4c.[34] The FTIR spectra were also recorded with bare and glutaraldehyde functionalised paper biosensors, which showed the appearance of prominent peaks at 3437 cm^{-1}, demonstrating the presence of NH stretching, OH stretching at 1640 cm^{-1} and 1562 cm^{-1} (amide II band), and 1420 cm^{-1} for CH_2 bending, respectively,[35] as illustrated in Fig. 4d.

3.3. Analytical performance of the biosensor

3.3.1 Optical sensing and parameter optimization studies. Since the detection is based on colorimetry, first, it is important to understand the role of all individual components in the optical signal of sensing probes. Hence, the absorbance was recorded for each component. Phenol red [PR], used as a pH

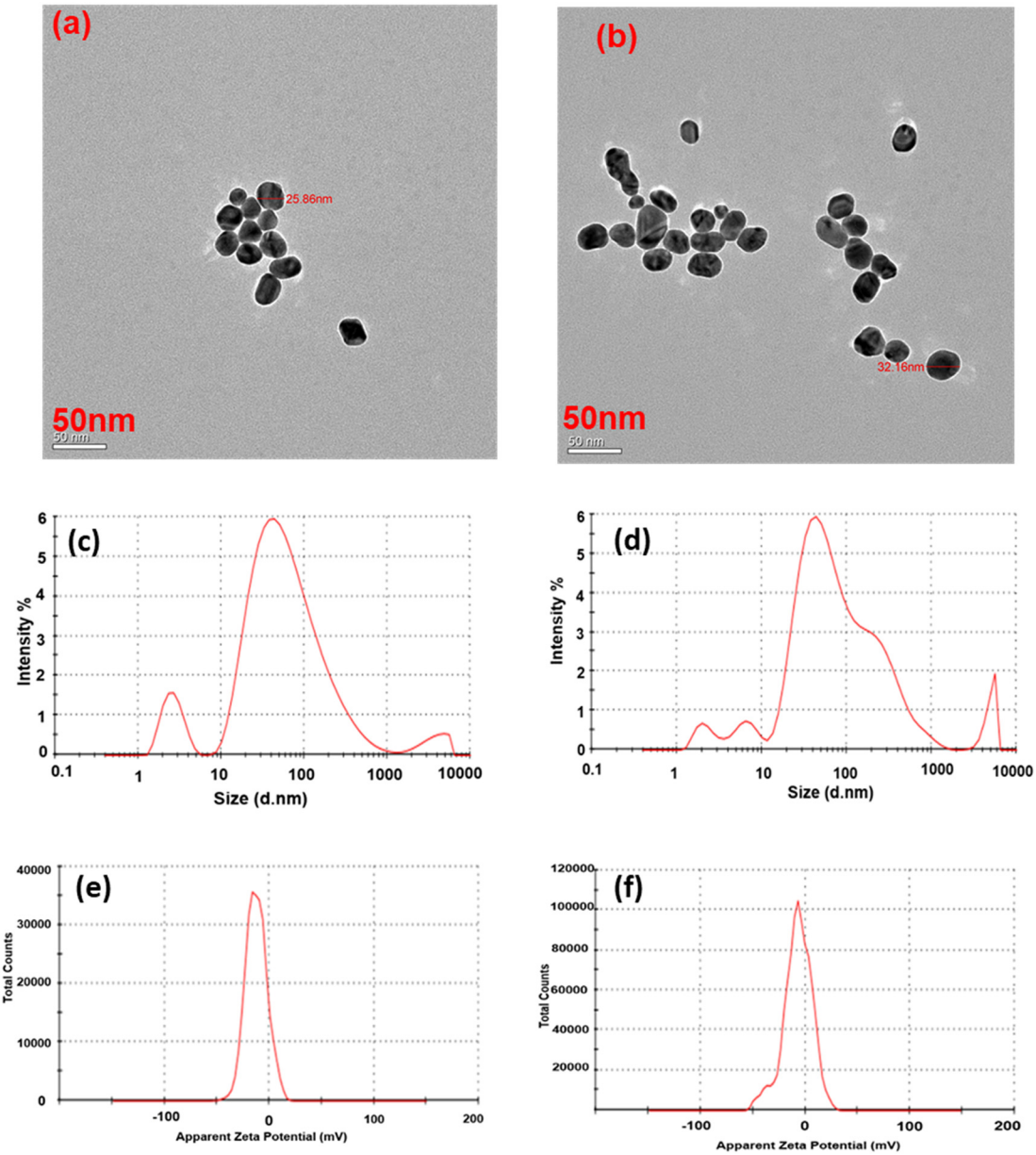

Fig. 3 (a and b) TEM images, (c and d) DLS measurements and (e and f) zeta potentials of AuNPs & AuNP@Ab conjugates.

indicator, exhibited absorbance peaks at 431 nm & 560 nm, respectively. The peak at 431 nm indicates its acidic nature, whereas the peak at 560 nm demonstrates its basic nature, which emerges due to loss of a proton from its ketone group. The protonated form of phenol red pH <6.8 exhibits yellow color; however, the transition phase from pH 6.8–8.2 shows change in the solution color from orange to red.[36] For sensing application, since the detection is based on the pH sensitivity of phenol red and most of the changes were towards the basic condition, the peak at 560 nm is used as a reference peak for monitoring the signal. Glutaraldehyde (Glu), which has been used as a fixing agent for bioreceptor attachment on paper biosensors, didn't show any peaks in the scanned range because of the presence of a double bond within the chromophore. However, subsequent to its addition to phenol red dye, the peak at 560 nm disappeared and the intensity of the peak at 431 nm decreased due to the acidic nature of glutaraldehyde with pH 3. A similar effect was observed on the addition of AuNP@Ab conjugates to phenol red–glutaraldehyde (Glu) cocktail solution (pH 4.5), but in contrast, when antigen osteopontin was added to this PR-Glu-AuNP@Ab cocktail solution, the peak at 560 nm again re-appeared due to a subsequent change in the pH of this reaction cocktail (pH 7). The addition of only AuNPs to phenol red solution didn't result in the disappearance of the peak at 560 nm though the intensity of both the peaks was affected, as shown in Fig. 5a. However, Fig. 5b demonstrates that the increased concentration of the biomarker (OPN) results in the enhancement of the absorbance peak intensity at 560 nm, reflecting a transition of pH shift towards the alkaline state during biomarker binding.

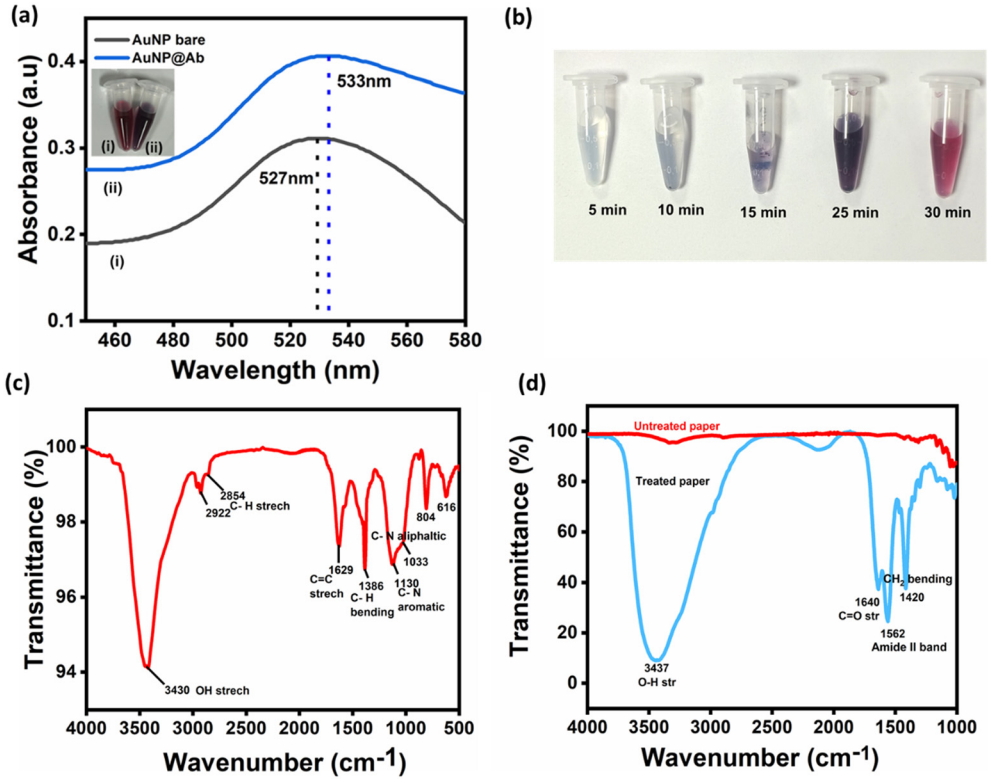

Fig. 4 (a) UV-vis absorbance spectra of the AuNPs & AuNP@Ab complex. (b) Change in reaction color with time. (c) FTIR spectrum of AuNPs. (d) FTIR spectra of untreated and glutaraldehyde-treated Whatman filter paper.

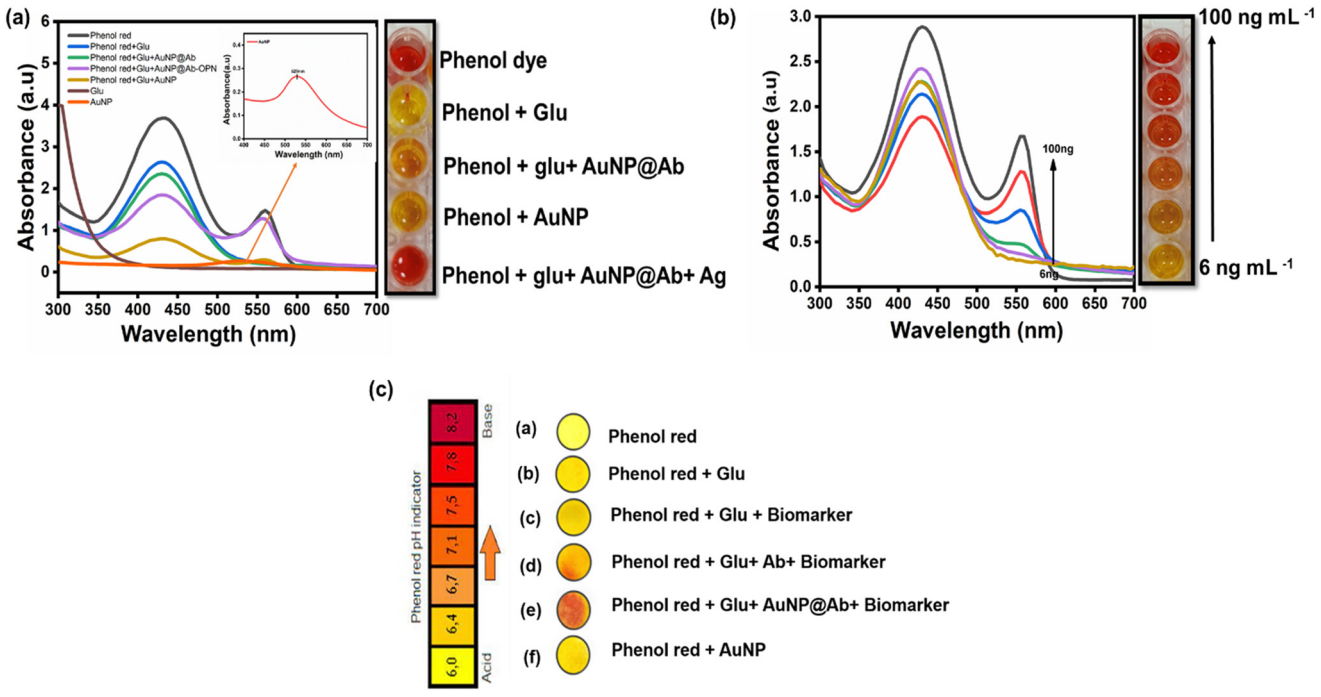

Fig. 5 (a) Absorbance spectra of different components of the biosensor, with respective color change in solution due to pH change. (b) Absorbance spectra of the biosensor as a function of osteopontin biomarker concentration. (c) Change in color of the test zone of the biosensor with different components of the biosensor on the paper.

After the study in solution form, this detection assay was shifted on the paper biosensor and recorded the change in the color of the test zone (Fig. 5c). Filter paper with phenol red appeared yellow in color, which on the addition to glutaraldehyde turned slightly dark due to the change in pH of the paper surface as glutaraldehyde (Glu) is acidic in nature, exhibiting pH between 3 and 4.5.[37] Likewise, various combinations were added on the paper biosensor to observe the role of each and every component in the developed paper biosensor (Fig. 5c). The PR-Glu-AuNP@Ab–Ag complex resulted in the change in the color of the test zone of the paper biosensor, which might be due to the change in the pH of phenol red on complex formation with the AuNP@Ab–Ag immunocomplex, wherein the gold nanoparticles have a tendency to agglomerate due to the change in the refractive index of the surrounding.[38] Phenol red serves as a biological indicator to monitor pH changes in the solution. Phenol red at a pH below 7 shows a yellow color, and at a pH above 7, it shows a red to pink color. The change in color of phenol red after antigen–antibody interactions suggests a significant change in pH, confirming the effectiveness of phenol red as an indicator in our analysis.

Further, the influence of parameters, *viz* pH, temperature, antigen–antibody concentration, reaction time and volume of gold nanoparticles, has also been studied. Since it is a paper biosensor, the optical response was recorded in the form of reflectance intensity.

Temperature optimization was also studied to enhance binding on the paper substrate. The AuNP@Ab complex, along with the OPN biomarker (100 ng mL^{-1}), was incubated at different temperatures (16 °C, 25 °C, 37 °C, 55 °C). The results demonstrate considerable variation in temperature on the binding affinity and stability of the interaction. As illustrated in Fig. 6a and b, it was concluded that 37 °C is the optimal temperature for the detection assay because temperatures below 37 °C reduce the binding affinity, reducing the molecular motion of the particle. However, temperatures above 40 °C decrease the antigen–antibody efficiencies, due to disturbed stability of the complex.[39] It was concluded that 37 °C is the optimal temperature for the detection assay, which shows a significant shift of 4 nm in the reflectance spectra from 533 nm to 537 nm after immunocomplex formation.

As mentioned in the discussion above on pH sensitivity of phenol red in the solution phase, similar behaviour is observed on the paper biosensor also, wherein only alkaline pH results in the change of phenol red color and consequently the peak at 560 nm is most significantly affected. In Fig. 7a, it can be seen that at pH 4 & 6, no peak is observed in the reflectance spectra. The peak at 545 nm was observed only for pH 7.0, which is consistent with the change in color of the test zone of the paper biosensor (Fig. 7a). The obtained color from the experiment is evaluated using ImageJ software, to calculate the mean of the RGB value as shown in Fig. 7b. RGB measurement helps in sensing the color difference by quantifying red, green, and blue light reflected and converting it into a numerical value. The darker the color shade, the lower the RGB value and *vice*

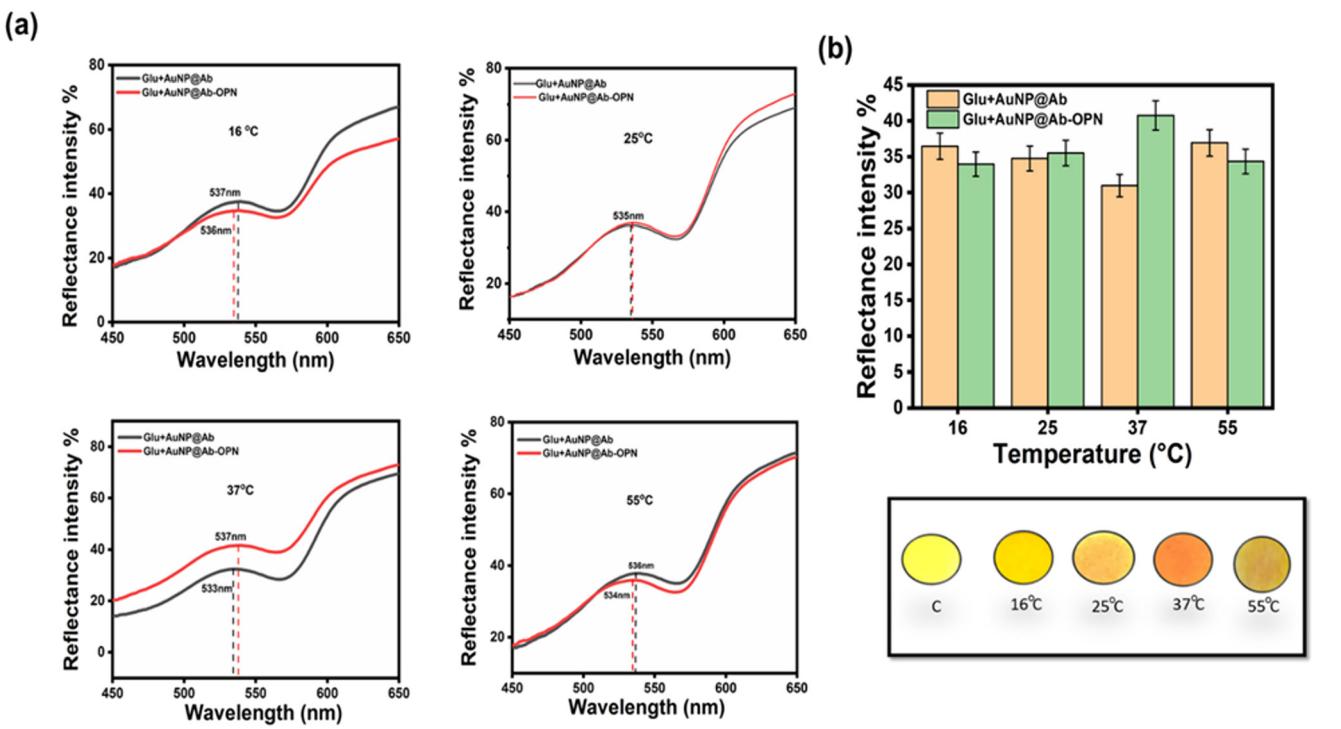

Fig. 6 Effects of temperature on (a) antigen (OPN)–antibody binding on the paper device. (b) Reflectance spectrum percentage & color variation in the test zone of the biosensor.

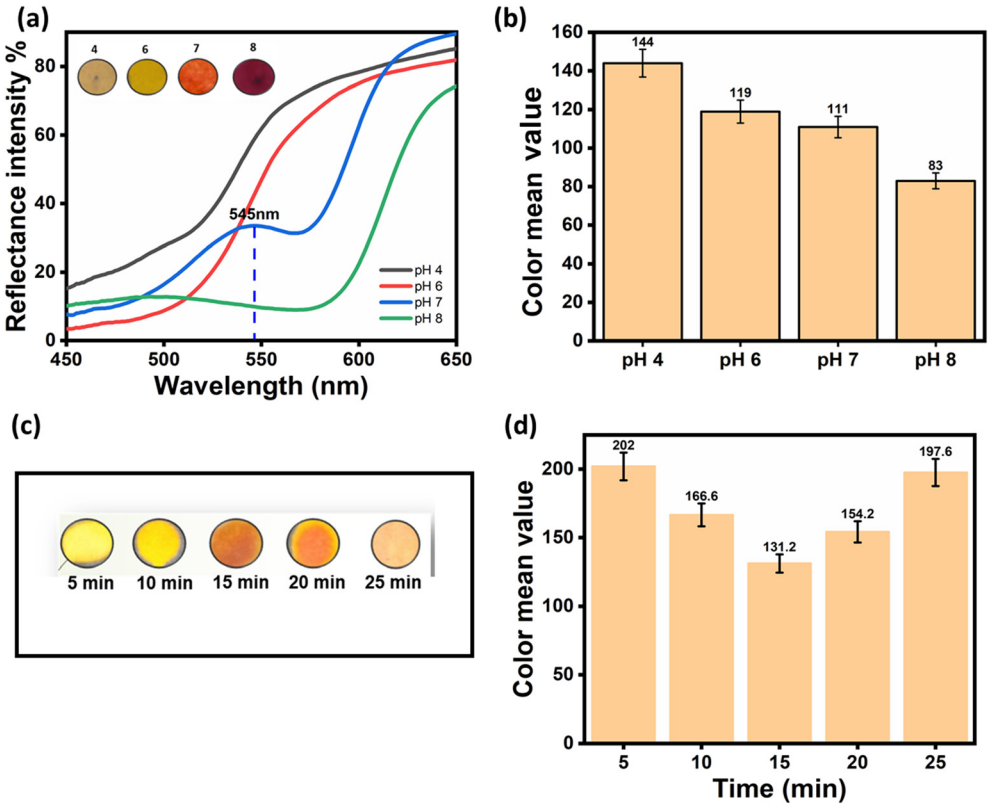

Fig. 7 (a) Reflectance spectra of the biosensor as a function of pH. (b) RGB values as a function of pH. (c) Visual colorimetric change in the color of the test zone of the developed biosensor. (d) Change in RGB color intensity (ImageJ software) as a function of incubation time.

versa. Based on these observations, the color shade obtained at pH 7.0 was used for monitoring the sensor signal, avoiding the color shade obtained at pH 8.0 since the antibodies are susceptible to damage at extreme alkaline pH. Exposure of antibodies to higher pH (>7) for a longer period of time alters their solubility and conformational integrity, and affects their interaction with the targeted biomarker, potentially destabilizing the protein structure.[40]

Incubation time was optimized using the same principle by varying incubation conditions for a reaction system. After dropping a sample on the paper, reaction times were monitored through color change by capturing the image for 5, 10, 15, 20, and 25 minute intervals as shown in Fig. 7c. The obtained color intensity was measured by using ImageJ software as the mean of RGB values as plotted in Fig. 7d. The results show that the reflectance color mean intensity is maximum at 15 min *i.e.*, the more intense color of the analyte corresponds to a lesser color mean value. Beyond 15 min of incubation, the color intensity start gradually decreased.

3.3.2 Paper-based detection of OPN in buffer. The paper-based biosensor is a promising tool with a simple design and lower cost and requires a small sample volume.[33] As a result, it has become popular among researchers working on biological and environmental applications. Following the protocol mentioned in the experimental section related to the development of the detection assay and the optimisation of input parameters, *viz* pH, temperature and incubation time, the biosensor was used for the detection of osteopontin antigen at varied antigen concentrations (1–125 ng mL^{-1}). The clinically reported cut off value for osteopontin concentration in osteoporosis diagnosis was 9.47 ng mL^{-1}, with a reported lower osteopontin level of 7.8 ng mL^{-1}. Based on the cut off value reported in the literature, a 1–125 ng mL^{-1} range has been selected for our measurement. The shade of the test zone changed from yellow at zero concentration to reddish-brown as the concentration of OPN increased (Fig. 8a). The reason for this is the change in pH of PR-treated paper during immunocomplex formation.

The mechanism behind the proposed work is that the glutaraldehyde-functionalized paper provides functional group accessibility for the binding of nanoparticle-conjugated antibodies over the paper surface *via* amine interactions. The addition of the antigen-AuNP@Ab complex induces local environmental changes at the paper surface. This network formation influences the protonation state of phenol red, resulting in a visible color transition from acidic (yellow) to alkaline (red).

Fig. 8b shows the change in the peak value as it goes from higher to lower concentration of antigen exposure, as compared to the peak value with no antigen. The resulting change in peak shift, as shown in Fig. 8b, occurs due to the binding of the antigen–antibody complex, which increases the overall size of the resulting complex. The colour intensity was further quantified by ImageJ software for a clear

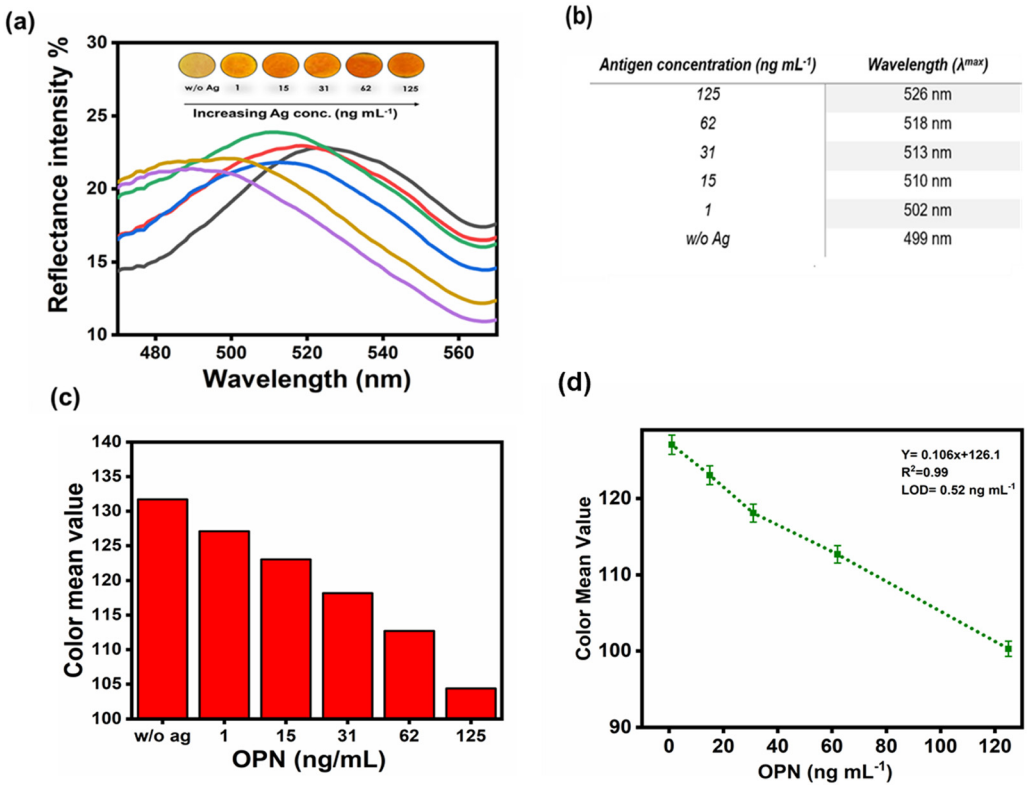

Fig. 8 (a) Reflectance study w.r.t. different Ag concentrations of OPN (1–125 ng mL^{-1}). (b) Change in the reflectance peak w.r.t. osteopontin biomarker concentration. (c) Color mean value variation observed at various OPN concentrations. (d) Linear fit graph.

distinction between the obtained color shades, which showed a linear regression value R^2 of 0.99 (Fig. 8c and d). The optimised performance metrics are summarised in Table 1. In addition to this, the response of the present biosensor has been compared with the response of other biosensors reported in the literature and is shown in Table 2. In comparison to other reported biosensors for osteoporosis biomarker estimation, the current platform offers enhanced advantages in term of sensitivity, response time, and operational simplicity, reduces sample processing and lowers instrumentation requirements. However, it still requires further work on long-term stability, comprehensive interference testing in diverse clinical samples, and expansion to multiplexed assays before it can fully match the broad capabilities offered by some commercially optimised systems.

3.3.3 Selectivity evaluation. One of the most important features of the device is to detect the target analyte with good characteristic performance. To assess selectivity, different other bone markers, including CTX-1, BSA, OSC, and OPN, were tested on the paper sensor and the reflectance intensity of each marker was recorded. Fig. 9(c) shows the targeted osteopontin (OPN) antigen showing a significant change in the color from yellow to red color as well as a decrease in the reflectance intensity value. Osteocalcin (OSC), BSA, and CTX-1 biomarkers did not show a statistically significant RGB color change and remained yellow. However, osteopontin (OPN) changed color from yellow to red, implying that our platform can detect osteopontin selectively.

We systematically evaluated the other interfering biomolecules, including glucose (1 mM), urea (1 mM), BSA + CTX + OSC (5 μg mL^{-1}), OPN alone (5 μg mL^{-1}), a mixture containing BSA + CTX + OSC + OPN (5 μg mL^{-1}), and ions Na^+, Ca^{2+}, and Zn (100 nM), at higher concentrations, as shown in Fig. 9(d). Our observations show that these components produce minimal color change, indicating a non-specific interaction, and that environmental factors do not influence the sensor response. In contrast, the osteopontin (OPN) and mixture (OPN, BSA + CTX + OSC) responses remain consistent and confirm OPN binding.

3.3.4 Sensor reproducibility and stability study. The reproducibility of the developed paper-based AuNP-antibody colorimetric sensor was verified to assess the consistency of the assay. For this, the sensor performance was measured

Table 1 Summarising key performance metrics

Targeted biomarker	Osteopontin
Material	Paper-based OPN/AuNP@Ab
Response time	15 min
Linear range	1–125 ng mL^{-1}
Detection limit	0.52 ng mL^{-1}

Table 2 Comparison of different detection methods reported in the literature

Detection method	Material	Biomarker	LOD	Linear range	Ref.
Electrochemical	SPGE modified/DNA aptasensor	Osteopontin	1.3 ± 0.1 nM	4.2 ± 1.1 nM	41
Colorimetric	Paper-based aptasensor	Osteopontin	5 ng mL^{-1}	5–1000 ng mL^{-1}	42
Electrochemical impedance spectroscopy	Gold electrode/modified 11-mercaptoundecanoic acid/6-mercapto-1-hexanol (MUA/MCH), DA and acetylated-HWRGWVA (HA-7)	Osteocalcin	0.17 nM	2.27–20.43 nM	43
Enzyme-free colorimetric	Osteocalcin/antibody-$Cu_3(PO_4)_2$ hybrid nanoflowers	Osteocalcin	0.042 ng mL^{-1}	0.1 to 50 ng mL^{-1}	44
Electrochemical impedance spectroscopy	Interdigital sensing surface using MIPs	CTX-1	0.09 ng mL^{-1}	0.1–3 ng mL^{-1}	45
Impedimetric immunosensor	Gold-coated carbon nanotube (CNT) control arrays for CTX-1 detection	CTX-1	0.05 ng mL^{-1}	0.05–0.4 ng mL^{-1}	46
Electrochemical impedance spectroscopy	Self assembled monolayer (SAM) dithiodiproponic acid deposit on a gold electrode	CTX-1	50 ng mL^{-1}	1–10 μg mL^{-1}	47
Colorimetric	Paper-based OPN/AuNP@Ab	Osteopontin	0.52 ng mL^{-1} in buffer and 0.48 ng mL^{-1} in serum	1–100 ng mL^{-1}	Our work

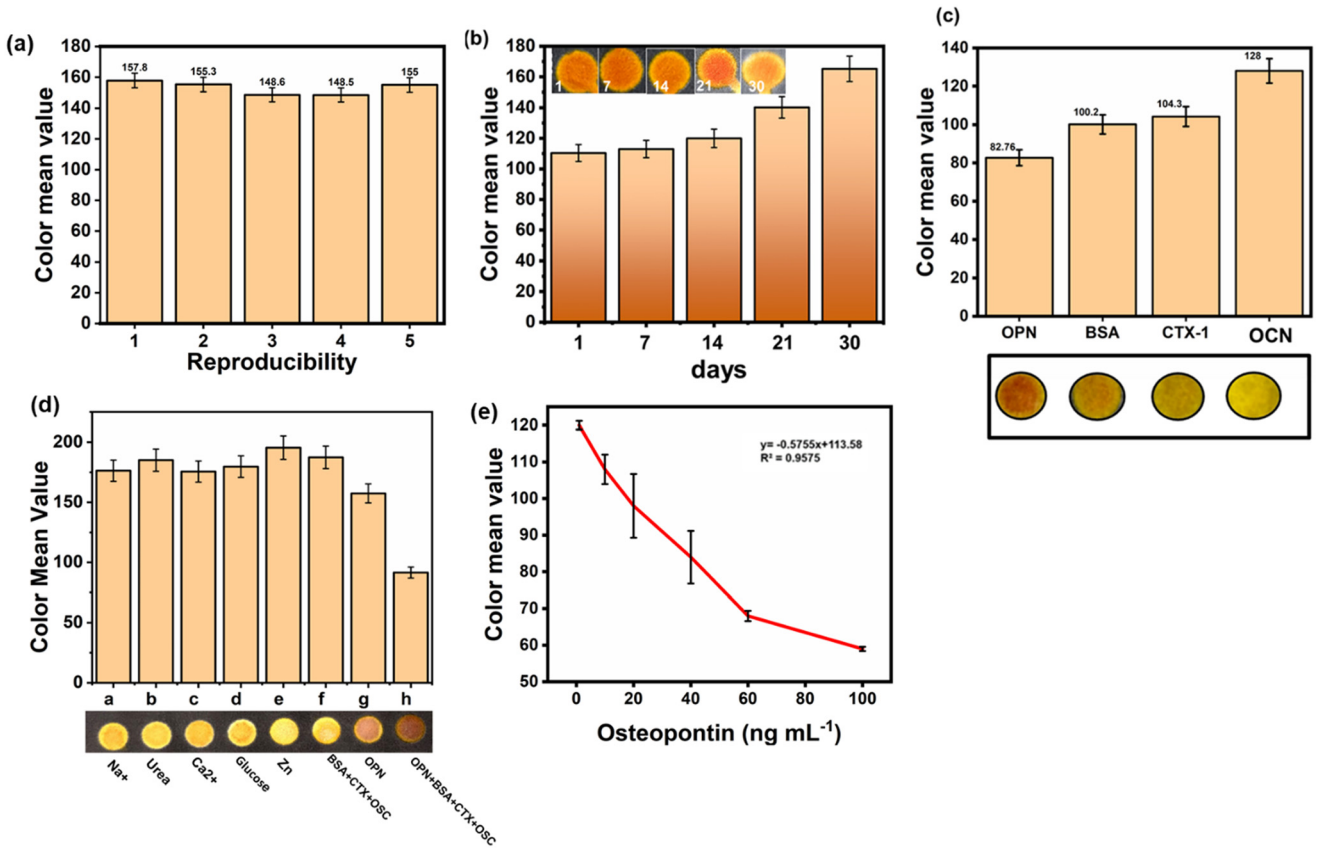

Fig. 9 (a) Sensor reproducibility. (b) Sensor stability. (c) Selectivity study. (d) Interference study. (e) Calibration curve for the osteopontin (OPN) biomarker in synthetic serum (mean value).

under the same conditions. The fabricated sensors were tested for the osteopontin (OPN) biomarker concentration of 10 ng mL^{-1} at pH 7.0 and 37 °C with an incubation time of 10–15 min following the same experimental protocol. The same experiment was conducted 5 consecutive times to ensure consistency of the assay. The resulting colorimetric response was quantified using RGB analysis as shown in Fig. 9(a). The sensor exhibits low variation in colour and high reproducibility, confirming consistency in sensing performance.

Table 3 A simple comparison of the most commonly used methods to measure bone turnover markers

Parameter	Developed paper-based OPN biosensor	DEXA (gold standard for osteoporosis diagnosis)	ELISA (gold standard for OPN quantification)
What it measures	Osteopontin (OPN)	Bone mineral density (BMD)	Osteopontin (OPN) in serum
Detection principle	Colorimetric change (phenol red) from pH shift induced by antigen–AuNP@Ab binding	Dual-energy X-ray attenuation	Antibody–antigen binding detected *via* an enzymatic chromogenic reaction
LOD	2.53 ng mL^{-1}	Not applicable to biomarkers	Typically 1–5 ng mL^{-1}
Detection time	10–15 minutes	10–20 minutes for scan	2–5 hours
Instrumentation	None	Large X-ray scanner	Microplate reader, centrifuge, lab setup
Cost per test	Very low	High	Moderate–high
Sample requirement	10–20 μL small serum volume	Full-body scan	50–100 μL serum
Use case	Point-of-care, early biochemical screening	Diagnosis of bone density loss	Laboratory quantification of OPN
Advantages	Portable, low-cost, rapid, suitable for community screening	Highly precise structural assessment of bone	Highly specific and quantitative
Limitations	Not a replacement for BMD measurement	Cannot detect biochemical changes	Time-consuming, multi-step, requires skilled operation

Similarly, the developed sensor's long-term stability was determined by monitoring its performance over 1, 7, 14, 21, and 30 days under similar controlled conditions. At each time, sensors were tested for the osteopontin biomarker at a concentration of 10 ng mL^{-1}, and the obtained colour responses were analysed through RGB. From Fig. 9(b), it was observed that the signal intensity remained consistent up to 14 days, indicating sensor stability during this period. However, a noticeable decline in signal reproducibility was observed at 21 and 30 days due to humidity and atmospheric oxygen; the test zone of the paper on which reagents were loaded reduces the activity of the antibodies due to detrimental conformation changes. The device demonstrates good short-term point-of-care performance at low cost and ease of fabrication, while future work focuses on extending its lifetime through material surface modification or a lyophilisation method to retain the activity of the antibody.

3.3.5 Performance evaluation in human spiked samples. The practical application of the developed biosensor is evaluated by detecting OPN in spiked human serum samples for a recovery study. In this, a known amount of OPN, such as 1–100 ng mL^{-1}, was spiked into a synthetic human serum. The color was then recorded, and the mean values of the red, green, and blue coordinates were determined using the ImageJ program. The linear plot graph of the obtained mean color intensity RGB values with respect to the change in concentration of the OPN was plotted, as shown in Fig. 9(e). The developed paper sensor can detect an LOD of 0.52 ng mL^{-1} in buffer and 0.48 ng mL^{-1} in commercial sera. The performance of the present biosensor is found to be better in terms of dynamic range and lower detection limit. The values of the limit of detection were calculated using the formula:

$$\text{Limit of detection (LOD)} = 3.3 \times \frac{\text{Standard deviation of response}}{\text{Slope of response}}$$

The recovery study for OPN in a spiked human serum sample with known amounts of OPN, such as 0, 10, 50, and 100 ng mL^{-1} were estimated. The color average RGB values of each concentration were determined. The obtained result of recovery percentage from samples ranged from 89% to 96% (Table 4), proving that the method is accurate and feasible for actual sample detection. Our proposed paper-based sensor is the first newly developed system, featuring minimal procedural step and has reduced analysis time. The performance comparison of the developed paper-based biosensor with the conventional diagnostic methods is shown in Table 3.

4 Conclusion

In our work, we developed a rapid, paper-based colorimetric detection assay for the osteopontin biomarker, which is considered one of the potential biomarkers in osteoporosis disease. It eliminates the need for sophisticated instruments, has a simple protocol, requires low operating costs, provides results within minutes and enables visual readout using a pH-responsive indicator. The assay mechanism is based on the binding of the gold nanoparticle-conjugated antibody complex to the osteopontin biomarker over the paper surface through glutaraldehyde functionality. Immunocomplex binding causes an increase in the size of the overall complex and a change in pH, which is evaluated by using phenol red dye. The proposed method is the first reported paper-based colorimetric OPN biomarker detection assay, which results in

Table 4 Sensor recovery obtained from spiked human serum samples

Sample	Average color intensity	Recovery (%)	RSD (%)
Blank	131.71	—	5.9
1	127.10	96.9	7.8
2	123.07	93.4	7.1
3	118.1	89.6	5.4

0.52 ng mL^{-1} detection limit in buffer and 0.48 ng mL^{-1} in synthetic serum. The use of AuNP–conjugates ensures selectivity, and the paper based platform supports portability and large-scale screening, making it highly suitable for point-of-care applications.

Author contributions

Amandeep Kaur (A. K): investigation, manuscript writing, revision corrections, review and editing. Suman Singh (S. S): supervision, conceptualization, finalization of the table of contents, drafting, guiding, editing, proof reading, funding and other lab support. Vikas: investigation, manuscript writing, review and editing. Sanjeev Soni: review and editing.

Conflicts of interest

The authors declare no conflict of interest.

Data availability

Data will be made available upon request.

Acknowledgements

The authors acknowledge the financial support received from the Indian Council of Medical Research (ICMR) for providing an ICMR-SRF Fellowship to A. K.

References

1 T. Sözen, L. Özışık and N. Ç. Başaran, An overview and management of osteoporosis, *Eur. J. Rheumatol. Inflammation*, 2016, **4**(1), 46.
2 N. S. Kadam, S. A. Chiplonkar, A. V. Khadilkar and V. V. Khadilkar, Prevalence of osteoporosis in apparently healthy adults above 40 years of age in Pune City, India, *Indian J. Endocrinol. Metab.*, 2018, **22**(1), 67–73.
3 E. E. Nagy, C. Nagy-Finna, H. Popoviciu and B. Kovács, Soluble biomarkers of osteoporosis and osteoarthritis, from pathway mapping to clinical trials: an update, *Clin. Interventions Aging*, 2020, 501–518.
4 H. B. Hetal Bhadricha, M. Khatkhatay and M. D. Meena Desai, Development of an in house ELISA for human intact osteocalcin and its utility in diagnosis and management of osteoporosis, *Clin. Chim. Acta*, 2019, **489**, 117–123.
5 S. Singh, D. Kumar and A. K. Lal, Serum osteocalcin as a diagnostic biomarker for primary osteoporosis in women, *J. Clin. Diagn. Res.*, 2015, **9**(8), RC04.
6 D. Fodor, C. Bondor, A. Albu, S.-p. Simon, A. Craciun and L. Muntean, The value of osteopontin in the assessment of bone mineral density status in postmenopausal women, *J. Invest. Med.*, 2013, **61**(1), 15–21.
7 X. Han, W. Wang, J. He, L. Jiang and X. Li, Osteopontin as a biomarker for osteosarcoma therapy and prognosis, *Oncol. Lett.*, 2019, **17**(3), 2592–2598.
8 F. Elefteriou, Regulation of bone remodeling by the central and peripheral nervous system, *Arch. Biochem. Biophys.*, 2008, **473**(2), 231–236.
9 J. Si, C. Wang, D. Zhang, B. Wang and Y. Zhou, Osteopontin in bone metabolism and bone diseases, *Med. Sci. Monit.*, 2020, **26**, e919159.
10 I.-C. Chang, T.-I. Chiang, K.-T. Yeh, H. Lee and Y.-W. Cheng, Increased serum osteopontin is a risk factor for osteoporosis in menopausal women, *Osteoporosis Int.*, 2010, **21**(8), 1401–1409.
11 T.-I. Chiang, I.-C. Chang, H.-S. Lee, H. Lee, C.-H. Huang and Y.-W. Cheng, Osteopontin regulates anabolic effect in human menopausal osteoporosis with intermittent parathyroid hormone treatment, *Osteoporosis Int.*, 2011, **22**(2), 577–585.
12 K. Wang, L. Yang, H. Huang, N. Lv, J. Liu and Y. Liu, Nanochannel array on electrochemically polarized screen printed carbon electrode for rapid and sensitive electrochemical determination of clozapine in human whole blood, *Molecules*, 2022, **27**(9), 2739.
13 Z. Yanyan, J. Lin, L. Xie, H. Tang, K. Wang and J. Liu, One-step preparation of nitrogen-doped graphene quantum dots with anodic electrochemiluminescence for sensitive detection of hydrogen peroxide and glucose, *Front. Chem.*, 2021, **9**, 688358.
14 J. P. Gosling, A decade of development in immunoassay methodology, *Clin. Chem.*, 1990, **36**(8), 1408–1427.
15 I. Kuronen, H. Kokko and M. Parviainen, Production of monoclonal and polyclonal antibodies against human osteocalcin sequences and development of a two-site ELISA for intact human osteocalcin, *J. Immunol. Methods*, 1993, **163**(2), 233–240.
16 J. Liu, X. Chen, H. Lv, S. He and Y. Fan, High-sensitivity immunoassay on interdigitated electrode to detect osteoporosis biological marker, *Biotechnol. Appl. Biochem.*, 2024, **71**(2), 256–263.
17 B. Yao, Z. Li, S. Wang, P. Anbu and J. Shao, Osteoporosis biomarker 'c-terminal telopeptide' identification on carbon nanofiber-modified interdigitated electrode sensor, *Appl. Phys. A: Mater. Sci. Process.*, 2022, 128.
18 Q. Chang, J. Huang, L. He and F. Xi, Simple immunosensor for ultrasensitive electrochemical determination of biomarker of the bone metabolism in human serum, *Front. Chem.*, 2022, **10**, 940795.
19 S. Kabala, H. Yagar and H. Özcan, A new biosensor for osteoporosis detection, *Prep. Biochem. Biotechnol.*, 2019, **49**, 1–10.
20 R. Chinnappan, N. S. Zaghloul, R. AlZabn, A. Malkawi, A. Abdel Rahman, K. M. Abu-Salah and M. Zourob, Aptamer selection and aptasensor construction for bone density biomarkers, *Talanta*, 2021, **224**, 121818.
21 Y. Chung and Y. Liu, Biosensor and method for bone mineral density measurement, *US Patent Application*, US20050059875A1, 2004.
22 L. Zhang, L. Liu and N. Xia, Electrochemical Sensing of Alkaline Phosphatase Activity Based on Difference of Surface Charge of Electrode, *Int. J. Electrochem. Sci.*, 2013, **8**(6), 8311–8319.

23 M. C. Hsieh, Y. K. Fang, M. S. Ju, J. J. Ho and S. F. Ting, Development of a new contact-type piezoresistive micro-shear-stress sensor, in *Design, Test, Integration, and Packaging of MEMS/MOEMS 2002*, SPIE, 2002, vol. 4755, pp. 285–295.
24 K. Kim, Y. Son, P.-S. Chang, J. Kim and H.-S. Jung, Design of a simple paper-based colorimetric biosensor using polydiacetylene liposomes for neomycin detection, *Analyst*, 2018, **143**(19), 4623–4629.
25 A. W. Martinez, S. T. Phillips, G. M. Whitesides and E. Carrilho, Diagnostics for the developing world: microfluidic paper-based analytical devices, *Anal. Chem.*, 2010, **82**(1), 3–10.
26 A. W. Martinez, S. T. Phillips, M. J. Butte and G. M. Whitesides, Patterned paper as a platform for inexpensive, low-volume, portable bioassays, *Angew. Chem.*, 2007, **119**(8), 1340–1342.
27 A. C. Pereira, F. T. C. Moreira, L. R. Rodrigues and M. G. F. Sales, Paper-based aptasensor for colorimetric detection of osteopontin, *Anal. Chim. Acta*, 2022, **1198**, 339557.
28 L. Shi, L. Wang, X. Yu, D. Kuang, Y. Huang and N. Yang, *et al.*, Colorimetric detection of furin based on enhanced catalytic activity of G-quadruplex/hemin DNAzyme, *Anal. Chim. Acta*, 2024, **1323**, 343070.
29 R. M. Yerrapragada and H. Narayanan Unni, based microfluidic device for diagnosis of osteoporosis markers, *Bioanalysis*, 2018, **10**(20), 1639–1649.
30 E. Celikbas, A. E. Ceylan and S. Timur, Paper-based colorimetric spot test utilizing smartphone sensing for detection of biomarkers, *Talanta*, 2020, **208**, 120446.
31 S. Yazdani, A. Daneshkhah, A. Diwate, H. Patel, J. Smith and O. Reul, *et al.*, Model for gold nanoparticle synthesis: Effect of pH and reaction time, *ACS Omega*, 2021, **6**(26), 16847–16853.
32 R. B. P. Rivera, R. B. Unabia, R. L. D. Reazo, M. A. Lapening, R. M. Lumod and A. G. Ruda, *et al.*, Influence of the gold nanoparticle size on the colorimetric detection of histamine, *ACS Omega*, 2024, **9**(31), 33652–33661.
33 M. Conrad, G. Proll, E. Builes-Münden, A. Dietzel, S. Wagner and G. Gauglitz, Tools to compare antibody gold nanoparticle conjugates for a small molecule immunoassay, *Microchim. Acta*, 2023, **190**(2), 62.
34 N. Niranjan Dhanasekar, G. Ravindran Rahul, K. Badri Narayanan, G. Raman and N. Sakthivel, Green chemistry approach for the synthesis of gold nanoparticles using the fungus Alternaria sp, *J. Microbiol. Biotechnol.*, 2015, **25**(7), 1129–1135.
35 S. Ramasubramaniam, C. Govindarajan, K. Nasreen and P. Sudha, Removal of cadmium (II) ions from aqueous solution using chitosan/starch polymer blend, *Compos. Interfaces*, 2014, **21**(2), 95–109.
36 M. Wang, S. Zhang, Z. Zhao, Z. Li, J. Nai and X. Liu, *et al.*, Phenol red hydrogel as pH indicator with protection against nanoceria degradation, *J. Sci.: Adv. Mater. Devices*, 2023, **8**(4), 100644.
37 T. Zhang, Z. Yu, Y. Ma, B.-S. Chiou, F. Liu and F. Zhong, Modulating physicochemical properties of collagen films by cross-linking with glutaraldehyde at varied pH values, *Food Hydrocolloids*, 2022, **124**, 107270.
38 M. J. Pollitt, G. Buckton, R. Piper and S. Brocchini, Measuring antibody coatings on gold nanoparticles by optical spectroscopy, *RSC Adv.*, 2015, **5**(31), 24521–24527.
39 R. W. Johnstone, S. M. Andrew, M. P. Hogarth, G. A. Pietersz and I. F. McKenzie, The effect of temperature on the binding kinetics and equilibrium constants of monoclonal antibodies to cell surface antigens, *Mol. Immunol.*, 1990, **27**(4), 327–333.
40 M. Hebditch, R. Kean and J. Warwicker, Modelling of pH-dependence to develop a strategy for stabilising mAbs at acidic steps in production, *Comput. Struct. Biotechnol. J.*, 2020, **18**, 897–905.
41 S. G. Meirinho, L. G. Dias, A. M. Peres and L. R. Rodrigues, Electrochemical aptasensor for human osteopontin detection using a DNA aptamer selected by SELEX, *Anal. Chim. Acta*, 2017, **987**, 25–37.
42 A. C. Pereira, F. T. Moreira, L. R. Rodrigues and M. G. F. Sales, based aptasensor for colorimetric detection of osteopontin, *Anal. Chim. Acta*, 2022, **1198**, 339557.
43 H. Chen, Q. Mei, S. Jia, K. Koh, K. Wang and X. Liu, High specific detection of osteopontin using a three-dimensional copolymer layer support based on electrochemical impedance spectroscopy, *Analyst*, 2014, **139**(18), 4476–4481.
44 W. Pan, T. Jiang, T. Lu, Q. Jin, Y. Xi and W. Zhang, Biomimetic-mineralized bifunctional nanoflowers for enzyme-free and colorimetric immunological detection of protein biomarker, *Talanta*, 2022, **238**, 123001.
45 N. Afsarimanesh, S. C. Mukhopadhyay and M. Kruger, Molecularly Imprinted Polymer-Based Electrochemical Biosensor for Bone Loss Detection, *IEEE Trans. Biomed. Eng.*, 2018, **65**(6), 1264–1271.
46 M. Ramanathan, M. Patil, R. Epur, Y. Yun, V. Shanov and M. Schulz, *et al.*, Gold-coated carbon nanotube electrode arrays: Immunosensors for impedimetric detection of bone biomarkers, *Biosens. Bioelectron.*, 2016, **77**, 580–588.
47 Y.-H. Yun, A. Bhattacharya, N. B. Watts and M. J. Schulz, A Label-Free Electronic Biosensor for Detection of Bone Turnover Markers, *Sensors*, 2009, **9**(10), 7957–7969.